



HAL
open science

DMRG study of the Berezinskii-Kosterlitz-Thouless transitions of the 2D five-state clock model

Christophe Chatelain

► **To cite this version:**

Christophe Chatelain. DMRG study of the Berezinskii-Kosterlitz-Thouless transitions of the 2D five-state clock model. 2014. hal-01035449v2

HAL Id: hal-01035449

<https://hal.science/hal-01035449v2>

Preprint submitted on 28 Aug 2014 (v2), last revised 11 Oct 2014 (v3)

HAL is a multi-disciplinary open access archive for the deposit and dissemination of scientific research documents, whether they are published or not. The documents may come from teaching and research institutions in France or abroad, or from public or private research centers.

L'archive ouverte pluridisciplinaire **HAL**, est destinée au dépôt et à la diffusion de documents scientifiques de niveau recherche, publiés ou non, émanant des établissements d'enseignement et de recherche français ou étrangers, des laboratoires publics ou privés.

DMRG study of the Berezinskii-Kosterlitz-Thouless transitions of the 2D five-state clock model

Christophe Chatelain

Groupe de Physique Statistique, Département P2M, Institut Jean Lamour
(CNRS UMR 7198), Université de Lorraine, France

E-mail: christophe.chatelain@univ-lorraine.fr

Abstract. The two Berezinskii-Kosterlitz-Thouless phase transitions of the two-dimensional 5-state clock model are studied on infinite strips using the DMRG algorithm. Because of the open boundary conditions, the helicity modulus Υ_2 is computed by imposing twisted magnetic fields at the two boundaries. Its scaling behavior is in good agreement with the existence of essential singularities with $\sigma = 1/2$ at the two transitions. The predicted universal values of Υ_2 are shown to be reached in the thermodynamic limit. The fourth-order helicity modulus is observed to display a dip at the high-temperature BKT transition, like the XY model, and shown to take a new universal value at the low-temperature one. Finally, the scaling behavior of magnetization at the low-temperature transition is compatible with $\eta = 1/4$.

PACS numbers: 05.20.-y, 05.50.+q, 75.10.Hk, 05.70.Jk, 05.10.-a

1. Introduction

The critical behavior of the two-dimensional XY model has been the subject of a huge literature. Because the symmetry group of the XY model is continuous, the Mermin-Wagner-Hohenberg theorem states that long-range order is destroyed by massless spin-wave excitations in dimension $d = 2$ [19, 11]. Therefore, in contrast to the Ising or 3 or 4-state Potts models, there cannot exist any ferromagnetic phase, where the symmetry would be spontaneously broken. However, at low temperature the two-dimensional XY model presents a critical phase that terminates at a topological Berezinskii-Kosterlitz-Thouless (BKT) phase transition where the coherence of spin waves is lost because of the proliferation of free topological defects [3, 14, 20]. BKT phase transitions were found in a variety of context, the superfluid transition of helium being certainly the most famous example of such a transition.

However, there exist situations where the Mermin-Wagner-Hohenberg theorem can be bypassed. For instance, the theorem extends to any kind of pair interaction but not to hard-core potentials [18]. As a consequence, a two-dimensional gaz of hard spheres crystallizes at low enough temperature. As the temperature is increased, the system undergoes two successive phase transitions separating, first the solid phase and an intermediate hexatic phase, and then, the hexatic and liquid phases [10]. The solid-hexatic phase transition is a BKT transition while the nature of the hexatic-liquid transition is controversial: it was long believed to be a BKT transition too but recent Monte Carlo simulations provided evidence of a first-order phase transition [4].

Another way to escape from the Mermin-Wagner-Hohenberg theorem is to replace the $U(1)$ symmetry of the XY model by a finite symmetry. This is the case of the q -state clock model, originally introduced by Potts [22]. The Hamiltonian is defined as

$$H_0 = - \sum_{\langle i,j \rangle} \cos \left(\frac{2\pi}{q} (\sigma_i - \sigma_j) \right), \quad \sigma_i \in \{0, \dots, q-1\} \quad (1)$$

where the sum extends over all pairs of nearest neighbors of the lattice. It is invariant under the \mathbb{Z}_q group of cyclic permutations of the q states. The XY model is recovered in the limit $q \rightarrow +\infty$. For $q \leq 4$, the two-dimensional clock model undergoes a unique second-order phase transition, like the Potts model. For $q \geq 5$, the phase diagram shows, between the ferromagnetic and paramagnetic phases, an intermediate critical phase with quasi long-range order [13]. These three phases are separated by two BKT phase transitions. The transition between the critical and paramagnetic phases occurs at a temperature roughly independent of q . The transition temperature of the second transition decays to zero as the number of states q goes to infinity, in agreement with the absence of ferromagnetic order predicted by the Mermin-Wagner-Hohenberg theorem for the 2D XY model. The situation is however not completely clear in the case $q = 5$. Early Monte Carlo simulations provided evidence of the existence of three distinct phases [24]. The average complex magnetization was shown to display the expected \mathbb{Z}_5 -symmetry in the ferromagnetic phase and a continuous $U(1)$ symmetry in the critical phase [6]. If the low-temperature transition was recognized as a BKT transition, the question of the nature of the high-temperature transition was subject to controversy in the last years. The claim that the high-temperature transition could not be of BKT-type for $q \leq 6$ [16] was supported by a study of Fisher zeroes [12]. However, recent Monte Carlo studies showed that the helicity modulus Υ_2 , defined as the response of the system to a twist [7], displays a jump, as expected in the case of a BKT transition [2, 5, 1, 15]. The observation of a non-vanishing helicity modulus in the high-temperature phase was explained as the result of an inappropriate definition of Υ_2 in the case of the clock model [15].

The helicity modulus is central in showing the BKT nature of the transition. However, because it is defined as a derivative of the free energy with respect to a twist, its computation is not straightforward in a Monte Carlo simulation. In the references mentioned above, the boundary-flip Monte Carlo method was employed [9]. In this paper, we present new results for the second and fourth-order helicity modulus of the 5 and 6-state clock models obtained using the Density Matrix Renormalization Group (DMRG) algorithm [25, 26, 23]. Details about the numerical calculations and the definition of the helicity modulus is presented in the second section. The numerical data are analyzed in the third section. The scaling behaviour of the helicity modulus, of the fourth-order helicity modulus and of magnetization are compared to Kosterlitz-Thouless predictions. Conclusions follow.

2. DMRG algorithm, observables and convergence

In this section, the DMRG algorithm is briefly presented. Our implementation and the simulation parameters are discussed. The definition of the estimator of the helicity modulus is given and finally, the convergence is studied.

From the Hamiltonian (1) on a square lattice, a transfer matrix is easily defined in the vector space of spin configurations on the last row of a strip of width L . The free

energy of the system is proportional to the logarithm of the largest eigenvalue of the transfer matrix. However, since the spins take q possible values, the dimension of this vector space grows as q^L , i.e. exponentially fast. In the case $q = 5$ we are interested in, this limits the strip widths that can be studied to small values, $L = 9$ or 10 . In the Density Matrix Renormalization Group (DMRG) approach, the system is divided into two blocks, left and right, and two central spins. The vector space is written as the tensor product of the vector spaces of each one of these three pieces. For a small system, the eigenvector of the transfer matrix associated to the largest eigenvalue can be computed exactly. Effective transfer matrices with a smaller dimensions are then constructed for the left and right blocks. As shown by White [25, 26, 23], the best approximation, in the sense of mean-square deviation of the eigenvector, is to truncate the basis of the left and right blocks by keeping only the eigenvectors associated to the largest eigenvalues of the reduced density matrix of the block. The central spins are then absorbed into the left and right blocks and two new spins are usually introduced between them. The procedure is repeated until the desired strip width is reached. This algorithm, called infinite-size DMRG, is efficient for homogeneous system. More details about the implementation of this algorithm can be found in the review [23]. In our case, we will introduce magnetic fields at the boundaries. Therefore, we proceeded differently: only one block, say left, is considered. The second block, say right, is reduced to a single spin. After the construction of an effective transfer matrix for the left block, new spins are not introduced between the former central spins but at the right of the right block. The procedure is iterated up to the desired strip width. The same algorithm is used to construct a sequence of effective transfer matrices for the right block. Once the final lattice size has been reached, the accuracy of the free energy can be further improved by applying several iterations of the finite-size DMRG algorithm. A sweep over the system is performed by increasing the length of one block and decreasing the length of the other one. We systematically performed six sweeps, in both directions. Even for the longest strips, the free energy was observed to reach a stable value (10 digits were considered), after three sweeps.

Since the DMRG algorithm gives directly access to the free energy, the helicity modulus Υ_2 can be calculated as

$$\Upsilon_2 = L^2 \left(\frac{\partial^2 f}{\partial \Delta^2} \right)_{\Delta=0} \quad (2)$$

where $f(\Delta)$ is the free energy density of the system when a twist Δ is introduced at its boundary. However, as emphasized by Kumano *et al.* [15], spins are not continuous in the clock model but takes a finite number of states so the twist can only be a multiple of $2\pi/q$. The usual definition of the helicity modulus should be replaced in this case by

$$\Upsilon_2 = \frac{2L^2}{(2\pi/q)^2} [f(2\pi/q) - f(0)]. \quad (3)$$

The twist is usually introduced in the system by replacing the interaction term in the Hamiltonian on one row by

$$- \cos \left(\frac{2\pi}{q} (\sigma_i - \sigma_j + 1) \right). \quad (4)$$

With periodic boundary conditions, a spin wave is induced to accommodate this interaction term. Unfortunately, periodic boundary conditions are known to greatly deteriorate the convergence of the DMRG algorithm. We therefore introduced a twist

by imposing magnetic fields at the two boundaries of an open system. The Hamiltonian now reads

$$H_{\Delta} = - \sum_{(i,j)} \cos\left(\frac{2\pi}{q}(\sigma_i - \sigma_j)\right) - \sum_{i \in S_L} \cos\left(\frac{2\pi}{q}\sigma_i\right) - \sum_{i \in S_R} \cos\left(\frac{2\pi}{q}\sigma_i - \Delta\right) \quad (5)$$

where S_L (resp. S_R) denotes the set of spins at the left (resp. right) boundary of the strip. Equivalently, the system can be seen as a strip of width $L + 2$ with spins frozen in the states $\sigma_i = 0$ and $\sigma_i = \frac{q}{2\pi}\Delta$ on the first and last rows respectively. The helicity modulus is determined as the finite difference of the free energy (3). We also tested the same definition but with a larger twist $\Delta = 4\pi/q$. Following [21], a fourth-order helicity modulus Υ_4 can be defined in the case of an infinitesimal twist Δ from the Taylor expansion

$$f(\Delta) = f(0) + \frac{\Delta^2}{2}\Upsilon_2 + \frac{\Delta^4}{4!}\Upsilon_4 + \mathcal{O}(\Delta^6) \quad (6)$$

of the free energy density. We introduced the estimator

$$\Upsilon_4 = \frac{2}{(2\pi/q)^4} [f(4\pi/q) + 3f(0) - 4f(2\pi/q)]. \quad (7)$$

Finally, since the \mathbb{Z}_q symmetry is broken, the spontaneous magnetization can be computed when $\Delta = 0$, i.e. when the magnetic fields at the two boundaries are aligned in the same direction.

In Monte Carlo simulations, error bars on any observable O are related to the fluctuations of O . According to the central limit theorem, the error on O is given by $\sqrt{\sigma_O^2 \tau / N}$ where σ_O^2 is the variance of O , N the number of Monte Carlo steps and τ the autocorrelation time. Error bars are therefore purely statistical and a better accuracy is reached by increasing the number of Monte Carlo steps. Systematic deviations arise only when the system was not properly thermalized or when the dynamics is not ergodic. In DMRG calculations, there is no statistical fluctuation of free energy around its exact value but only systematic deviations due to the truncation of the vector spaces of the left and right blocks. These deviations are difficult to estimate. In the following, the convergence of the helicity modulus is studied at the inverse temperature $\beta = 1/k_B T = 1.08$, i.e. $T \simeq 0.925$. This temperature roughly lies at the center of the critical phase of the 5-state clock model. It is therefore the most difficult case for numerical simulations. Since the correlation length is expected to diverge with the lattice size in this phase, the left and right blocks are strongly correlated through the two central spins. As a consequence, the reduced density matrix is observed to have a slowly decaying spectrum. Because the deviation of free energy is expected to be proportional to the sum of the eigenvalues of the reduced density matrix associated to the eigenvectors that have been discarded [17], each truncation of the basis of the two blocks leaves an effective transfer matrix that may reproduce poorly these correlations if a too small number of states is kept.

On figure 1, the helicity modulus is plotted versus the number of states m kept after truncation. More precisely, m refers to the number of states describing both the left (resp. right) block and the left (resp. right) central spin after the renormalization step. The dimension of the full vector space is therefore m^2 . For the smallest lattice sizes, the numerical data do not show any dependence on m . However, the free energy displays a small evolution at the 8th digit for $L \geq 64$. Since the helicity modulus Eq. 3 is defined as the difference of two free energies, the deviation is larger for Υ_2 . Indeed, for $L = 64$, the free energies are of order $\mathcal{O}(10^4)$ while their difference is of order

$\mathcal{O}(10^0)$. As a consequence, an evolution of Υ_2 with m is observed at the 4th digit for $L = 64$ and at the third one for $L = 256$. To quantify the systematic deviation of our data, we extrapolated them to the limit $m \rightarrow +\infty$. As observed for instance in the case of $SU(N)$ chains [8], the free energy is well described by a power law decay $f(m) = f(\infty) + am^{-\alpha}$ with $\alpha \simeq 4$. The helicity modulus Υ_2 is also reasonably well fitted by such a law, though other laws, in particular $\Upsilon_2(m) = \Upsilon_2(\infty) + ae^{-m/m_0}$ with $m_0 \simeq 70$, give sensibly similar results. At $L = 256$, the fit is moreover hampered by the existence of oscillations that becomes more and more important at large lattice sizes. At $L = 128$ and $\beta = 1.08$, the helicity modulus can be extrapolated to the value 0.86450 (with both power-law and exponential fits) in the limit $m \rightarrow +\infty$. In the following, $m = 325$ states will be kept at each truncation. Since the helicity modulus takes the value 0.86453 for $m = 325$, the systematic deviation at $L = 128$ can be estimated to be of order $\mathcal{O}(10^{-5})$. By the same procedure, the deviation is shown to be one order of magnitude smaller for $L = 64$. For $L = 256$, this systematic deviation is of order $\mathcal{O}(10^{-4})$. In the following, numerical data for the 6-state clock will also be presented for comparison. For this model, $m = 648$ states were kept during the truncations but lattice sizes only up to $L = 64$ could be considered.

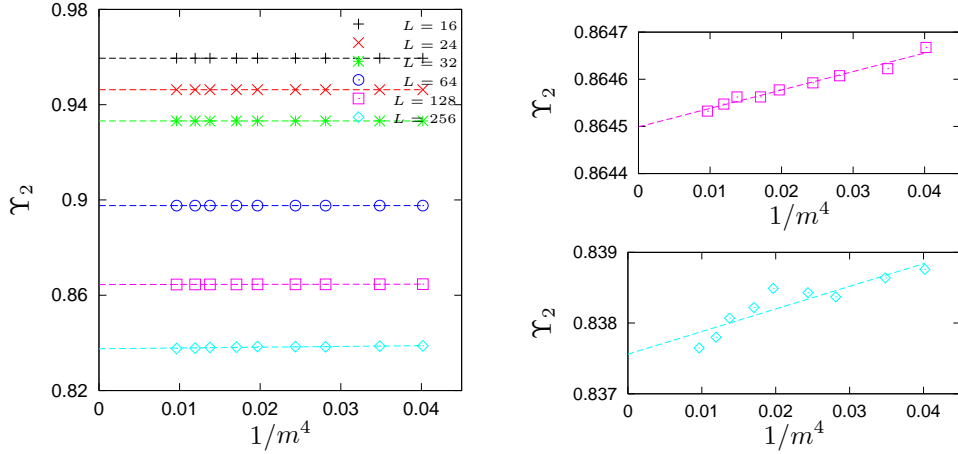


Figure 1. Helicity modulus Υ_2 of the 5-state clock model at the inverse temperature $\beta = 1/k_B T = 1.08$ versus $1/m^4$ where m is the number of states of the truncated vector spaces of the left and right blocks during the DMRG process. The different curves correspond to different lattice sizes L and the straight lines to linear fits. On the right, a zoom is performed on the curves for $L = 128$ (top) and $L = 256$ (bottom).

3. Numerical evidence of two BKT transitions

3.1. Helicity modulus

A clear signature of the BKT transitions is provided by the helicity modulus Υ_2 . The temperature dependence of Υ_2 is plotted on figure 2 for both the 5 and 6-state clock models. In the ferromagnetic phase, the twist imposed at the boundaries induces domain walls rather than spin waves. As a consequence, $L[f(\Delta) - f(0)]$ is finite. Since the helicity modulus is proportional to $L^2[f(\Delta) - f(0)]$, it diverges in the

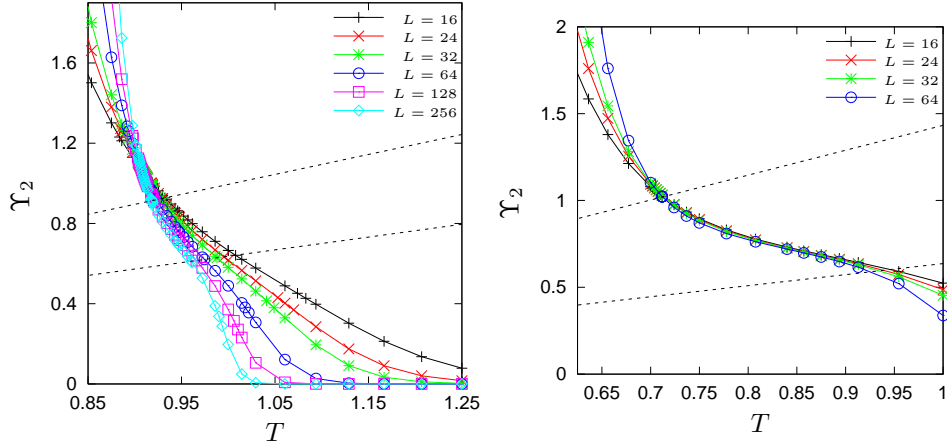


Figure 2. On the left, helicity modulus Υ_2 of the 5-state clock model versus the temperature T for different lattice sizes L . The two dashed lines correspond to the predicted RG relations at the BKT transition temperatures. On the right, the helicity modulus of the 6-state clock model is plotted for comparison.

ferromagnetic phase, as can be observed on the figure. In the paramagnetic phase, the correlation length is finite so no (quasi) long-range order can propagate into the system and the difference $L[f(\Delta) - f(0)]$, as well as the helicity modulus, goes to zero as the lattice size is increased. For large lattice sizes, the helicity modulus is perfectly equal to zero, in contradistinction to previous claims. In the critical phase, the helicity modulus is expected to take a size-independent value. If this behavior is clearly observed on figure 2 for the 6-state clock model, this is not yet the case for the 5-state model, even though the curves come closer to each other as the lattice size is increased. The two expected jumps of helicity modulus are not observed yet but the tangent of the curve becomes more and more steep at temperatures close to the expected BKT transition temperatures $T_{\text{BKT}}^{\text{low}} \simeq 0.90$ and $T_{\text{BKT}}^{\text{high}} \simeq 0.95$.

When the BKT transition point is approached from the non-critical phase, the helicity modulus takes a universal value which is predicted to be proportional to T_{BKT} . In the case of the 2D clock model, these two universal quantities are [15]:

$$\Upsilon_2(T_{\text{BKT}}^{\text{high}}) = \frac{2}{\pi} T_{\text{BKT}}^{\text{high}}, \quad \Upsilon_2(T_{\text{BKT}}^{\text{low}}) = \frac{q^2}{8\pi} T_{\text{BKT}}^{\text{low}}. \quad (8)$$

These linear behaviors are plotted on figure 2. The different curves are expected to intersect each one of these two straight lines at the same point in the thermodynamic limit. As can be seen on the figure, and as already noted by Kumano *et al.* [15], this is not yet the case in the range of lattice sizes that were considered. However, the accuracy of the DMRG data allows to determine the intersection of the helicity modulus with the two predictions (8). On figure 3, the temperatures at which occur these intersections are plotted versus $1/(\ln L)^2$. Since the correlation length displays an essential singularity

$$\xi \sim e^{a|T - T_{\text{BKT}}|^{-1/2}}, \quad T > T_{\text{BKT}} \quad (9)$$

the temperature shift $T - T_{\text{BKT}}$ should indeed scale as $1/(\ln L)^2$ in the Finite-Size regime $\xi \sim L$. The data are in good agreement with this statement. Linear fits lead then to the

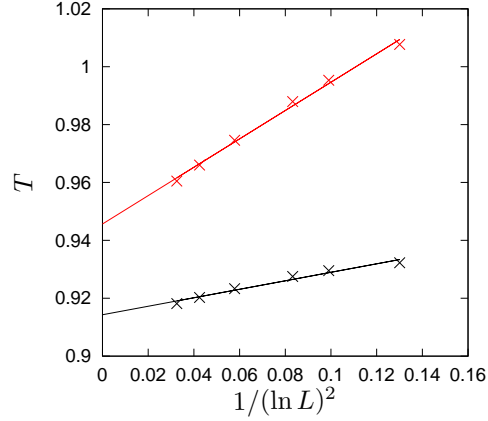


Figure 3. Temperatures where the helicity modulus Υ_2 of the 5-state clock model intersects the Renormalization Group predictions (8) versus $1/(\ln L)^2$. L is the width of the strip. The straight lines are linear fits.

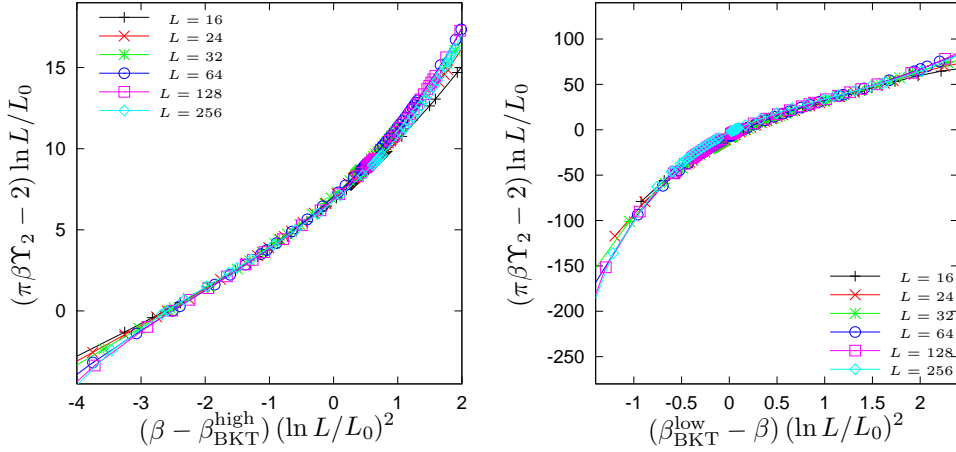


Figure 4. Scaling function \mathcal{F}_Υ (up to a factor) of the 5-state clock model with respect to the scaling argument $(\beta_{\text{BKT}} - \beta) (\ln L/L_0)^2$. The different symbols correspond to different lattice sizes. The left figure corresponds to the high-temperature BKT transition while the right one corresponds to the low-temperature transition.

extrapolated BKT transition temperatures $T_{\text{BKT}}^{\text{low}} \simeq 0.914(12)$ and $T_{\text{BKT}}^{\text{high}} \simeq 0.945(17)$, in agreement with earlier estimates $T_{\text{BKT}}^{\text{low}} \simeq 0.90514(9)$ and $T_{\text{BKT}}^{\text{high}} \simeq 0.95147(9)$ [6] obtained by other, more accurate, techniques but not involving the helicity modulus.

A stronger prediction of Kosterlitz-Thouless theory is that the universal value of the helicity modulus is approached as

$$\Upsilon_2(T) - \Upsilon_2(T_{\text{BKT}}) \sim \left[\ln \frac{L}{L_0} \right]^{-1} \mathcal{F}_\Upsilon(|T - T_{\text{BKT}}| (\ln L/L_0)^2) \quad (10)$$

where \mathcal{F}_Υ is a universal scaling function. This prediction is tested on figure 4 for the two BKT transitions of the clock model. The collapse of the curves is reasonably good

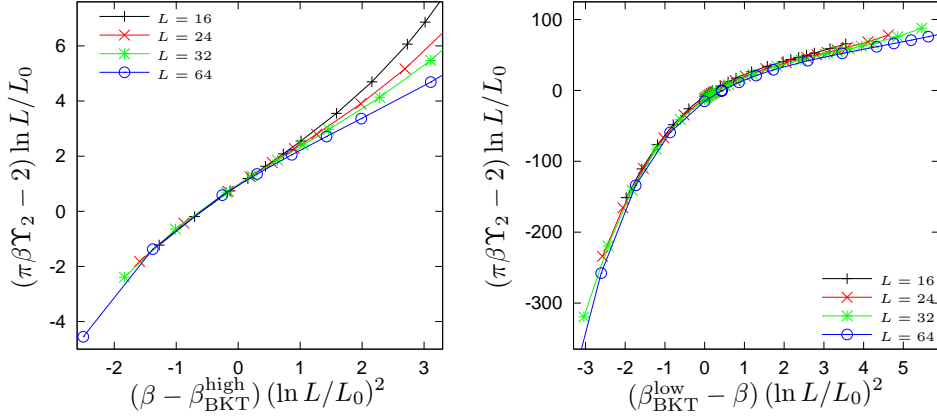


Figure 5. Scaling function \mathcal{F}_Υ (up to a factor) of the 6-state clock model with respect to the scaling argument $(\beta_{\text{BKT}} - \beta) (\ln L/L_0)^2$. The different symbols correspond to different lattice sizes. The left figure corresponds to the high-temperature BKT transition while the right one corresponds to the low-temperature transition.

for a wide range of the scaling parameter. For comparison, the same curves are plotted for the 6-state clock model on figure 5. In the case $q = 5$, the transition temperatures $T_{\text{BKT}}^{\text{low}}$ and $T_{\text{BKT}}^{\text{high}}$ were treated, like L_0 , as free parameters. The best values were defined as the minimum of the square deviation around the mean over the different lattice sizes. The collapse on figure 4 was obtained with $T_{\text{BKT}}^{\text{low}} \simeq 0.917$ and $L_0 \simeq 0.87$ at the low temperature BKT transition and $T_{\text{BKT}}^{\text{high}} \simeq 0.927$ and $L_0 \simeq 0.07$ at the second transition. These values are still relatively different with the estimates of $T_{\text{BKT}}^{\text{low}}$ and $T_{\text{BKT}}^{\text{low}}$. However, these values are very sensible to the interval of temperatures on which the mean-square deviation is minimized. Almost as good collapses can be obtained with the temperatures $T_{\text{BKT}}^{\text{low}} \simeq 0.90514(9)$ and $T_{\text{BKT}}^{\text{high}} \simeq 0.95147(9)$ [6]. In the case $q = 6$ plotted on figure 5, we restricted ourselves to use the same values as in Ref. [15].

3.2. Fourth-order helicity modulus

As shown by Kim *et al.* in the case of the XY model [21], the discontinuity of the helicity modulus Υ_2 at the BKT transition temperature manifests itself as a dip in higher-order derivatives of the free energy density. The temperature dependence of the fourth-order helicity modulus Υ_4 , estimated as (7), is plotted on figure 6. Like the helicity modulus Υ_2 , it vanishes in the high temperature phase. The formation of a dip is clearly seen around $T_{\text{BKT}}^{\text{high}}$. However, the low-temperature BKT transition does not manifest itself as a dip. Nevertheless, it seems that the intersection of the curves at temperatures close to $T_{\text{BKT}}^{\text{low}}$ indicates that Υ_4 takes a universal value, like Υ_2 , at $T_{\text{BKT}}^{\text{low}}$ rather than displaying a dip. On the right figure, the location of the dip and the temperatures at which the curves intersect for two successive lattice sizes are plotted versus $1/(\ln L)^2$. Both can only be roughly determined but, nevertheless, a linear behavior is observed if one excludes the point $L = 16$. Linear fits give the BKT transition temperatures $T_{\text{BKT}}^{\text{low}} \simeq 0.91(2)$ and $T_{\text{BKT}}^{\text{high}} \simeq 0.96(4)$, again in agreement with earlier estimates $T_{\text{BKT}}^{\text{low}} \simeq 0.90514(9)$ and $T_{\text{BKT}}^{\text{high}} \simeq 0.95147(9)$ [6].

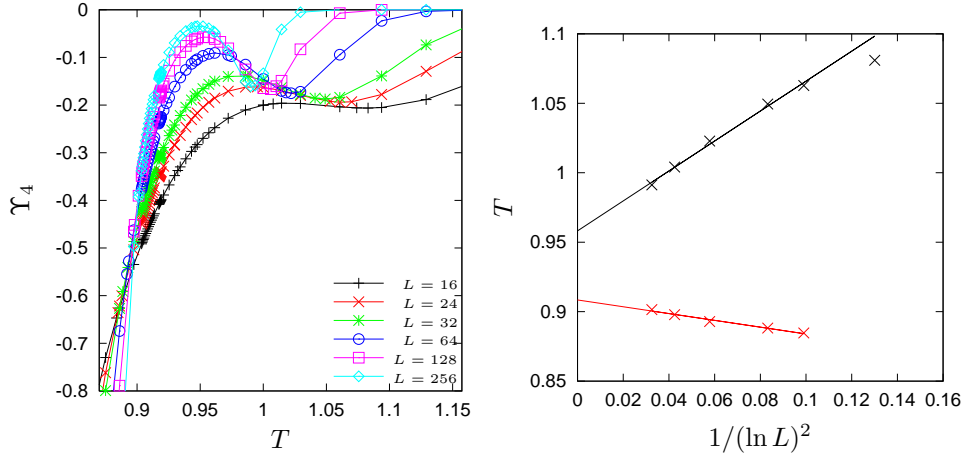


Figure 6. On the right, fourth derivative Υ_4 of the free energy density (Eq. 7) of the 5-state clock model versus temperature T . The different curves correspond to different lattice sizes L . The two BKT transitions are signaled by respectively the crossing of the curves and the dip. On the left, temperatures at which the intersection of the curves are observed (red) and location of the dip (black) versus $1/(\ln L)^2$. The straight lines are linear fits.

3.3. Magnetization

Even though the system is infinite in the longitudinal direction of the strip, a finite spontaneous magnetization is observed because magnetic fields are applied at the boundaries. The magnetization m is measured on the site $L/2$, i.e. at the center of the strip. The data are plotted on figure 7. In the scaling regime $L \gg \xi$, m is expected to display an essential singularity $\xi^{-\eta/2}$ while, in the finite-size regime, the usual algebraic law with the lattice size, $m \sim L^{-\beta/\nu}$ with $\beta/\nu = \eta/2$, is recovered. The magnetic scaling dimension is usually conjectured to take the same value as in the XY model, i.e. $\eta = 1/4$, even though recent Monte Carlo simulations systematically led to smaller values [6]. On figure 7, the scaling hypothesis

$$m \sim L^{-\eta/2} \mathcal{F}_m(|T - T_{\text{BKT}}| (\ln L/L_0)^2) \quad (11)$$

is tested with the value $\eta/2 = 1/8$. The collapse of the curves corresponding to different lattice sizes on figure 7 (right) shows that the scaling function \mathcal{F}_m depends, as expected, only on $|T - T_{\text{BKT}}| (\ln L/L_0)^2$. Again, the mean-square deviation was minimized to find to optimal values of the free parameters $T_{\text{BKT}}^{\text{low}}$ and L_0 . The values $T_{\text{BKT}}^{\text{low}} \simeq 0.917$ and $L_0 \simeq 0.023$ were obtained. As in the case of the helicity modulus, small joint variations of these parameters lead to almost as good collapses so the method is not reliable to determine $T_{\text{BKT}}^{\text{low}}$ accurately. However, it provides evidence of the scaling behavior (11). We also tried to extract the magnetic exponent $\eta/2$ from a fit of magnetization as $m \sim L^{-\eta/2}$. At the temperature $T_{\text{BKT}}^{\text{low}} \simeq 0.90514$, the estimated exponent is $0.116(4)$, i.e. slightly below the expected value $1/8$. However, it increases with temperature, which suggests that strong scaling corrections are present. Using the temperature $T_{\text{BKT}}^{\text{low}} \simeq 0.917$ that leads to the best scaling Eq. 11, the exponent takes the value $\eta/2 = 0.1254(30)$, in perfect agreement with the expected value.

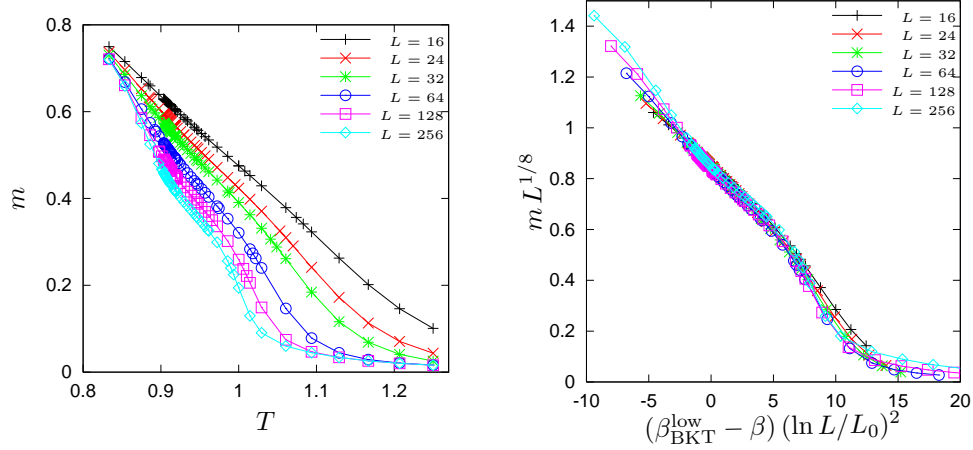


Figure 7. On the left, magnetization density m of the 5-state clock model versus the temperature T for different lattice sizes L . On the right, the scaling function $m L^{1/8}$ is plotted with respect to the scaling parameter $(\beta_{\text{BKT}}^{\text{low}} - \beta) (\ln L/L_0)^2$.

4. Conclusions

The two BKT phase transitions of the 5-state clock model were studied using the DMRG algorithm. The latter is shown to allow for larger lattice sizes with a better accuracy than Monte Carlo simulations. Despite the Open Boundary Conditions imposed by the technique, the helicity modulus Υ_2 , as well as higher-derivative Υ_4 , can be computed by imposing twisted magnetic fields on the two boundaries of the strip. The topological nature of the two phase transitions is confirmed. Finite-Size displacements of the BKT transition temperatures scale as $1/(\ln L)^2$, in agreement with an essential singularity of the correlation length. The exponent σ is therefore the same as for the XY model for both BKT transitions. The helicity modulus is shown to tend towards the universal values predicted by Renormalization Group techniques at the temperatures compatible with the most accurate Monte Carlo estimates. Finally, the scaling behavior of magnetization is also compatible with an essential singularity with the same magnetic scaling dimension $\eta/2 = 1/8$ as the XY model.

References

- [1] S. K. Baek, H. Mäkelä, P. Minnhagen, and B. J. Kim. Residual discrete symmetry of the five-state clock model. *Phys. Rev. E*, 88:012125, Jul 2013.
- [2] S. K. Baek and P. Minnhagen. Non-kosterlitz-thouless transitions for the q -state clock models. *Phys. Rev. E*, 82:031102, Sep 2010.
- [3] V. L. Berezinskii. *Zh. Eksp. Teor. Fiz.*, 61:1144, 1971.
- [4] E. P. Bernard and W. Krauth. Two-step melting in two dimensions: First-order liquid-hexatic transition. *Phys. Rev. Lett.*, 107:155704, Oct 2011.
- [5] O. Borisenko, V. Chelnokov, G. Cortese, R. Fiore, M. Gravina, and A. Papa. Phase transitions in two-dimensional $z(n)$ vector models for $n > 4$. *Phys. Rev. E*, 85:021114, Feb 2012.
- [6] O. Borisenko, G. Cortese, R. Fiore, M. Gravina, and A. Papa. Numerical study of the phase transitions in the two-dimensional $z(5)$ vector model. *Phys. Rev. E*, 83:041120, Apr 2011.
- [7] M. E. Fisher, M. N. Barber, and D. Jasnow. Helicity modulus, superfluidity, and scaling in isotropic systems. *Phys. Rev. A*, 8:1111–1124, Aug 1973.

- [8] M. Fhringer, S. Rachel, R. Thomale, M. Greiter, and P. Schmitteckert. Dmrg studies of critical su(n) spin chains. *Annalen der Physik*, 17(12):922–936, 2008.
- [9] A. P. Gottlob and M. Hasenbusch. The xy model and the three-state antiferromagnetic potts model in three dimensions: Critical properties from fluctuating boundary conditions. *Journal of Statistical Physics*, 77(3-4):919–930, 1994.
- [10] B. I. Halperin and David R. Nelson. Theory of two-dimensional melting. *Phys. Rev. Lett.*, 41:121–124, Jul 1978.
- [11] P. C. Hohenberg. Existence of long-range order in one and two dimensions. *Phys. Rev.*, 158:383–386, Jun 1967.
- [12] C.-O. Hwang. Six-state clock model on the square lattice: Fisher zero approach with wang-landau sampling. *Phys. Rev. E*, 80:042103, Oct 2009.
- [13] J. V. José, L. P. Kadanoff, S. Kirkpatrick, and D. R. Nelson. Renormalization, vortices, and symmetry-breaking perturbations in the two-dimensional planar model. *Phys. Rev. B*, 16:1217–1241, Aug 1977.
- [14] J. M. Kosterlitz and D. J. Thouless. Ordering, metastability and phase transitions in two-dimensional systems. *Journal of Physics C: Solid State Physics*, 6(7):1181, 1973.
- [15] Y. Kumano, K. Hukushima, Y. Tomita, and M. Oshikawa. Response to a twist in systems with Z_p symmetry: The two-dimensional p -state clock model. *Phys. Rev. B*, 88:104427, Sep 2013.
- [16] C. M. Lapilli, P. Pfeifer, and C. Wexler. Universality away from critical points in two-dimensional phase transitions. *Phys. Rev. Lett.*, 96:140603, Apr 2006.
- [17] Örs Legeza and Gábor Fáth. Accuracy of the density-matrix renormalization-group method. *Phys. Rev. B*, 53:14349–14358, Jun 1996.
- [18] N. D. Mermin. Crystalline order in two dimensions. *Phys. Rev.*, 176:250–254, Dec 1968.
- [19] N. D. Mermin and H. Wagner. Absence of ferromagnetism or antiferromagnetism in one- or two-dimensional isotropic heisenberg models. *Phys. Rev. Lett.*, 17:1133–1136, Nov 1966.
- [20] P. Minnhagen. The two-dimensional coulomb gas, vortex unbinding, and superfluid-superconducting films. *Rev. Mod. Phys.*, 59:1001–1066, Oct 1987.
- [21] P. Minnhagen and B. J. Kim. Direct evidence of the discontinuous character of the kosterlitz-thouless jump. *Phys. Rev. B*, 67:172509, May 2003.
- [22] R. B. Potts. Some generalized order-disorder transformations. *Mathematical Proceedings of the Cambridge Philosophical Society*, 48:106–109, 1 1952.
- [23] U. Schollwöck. The density-matrix renormalization group. *Rev. Mod. Phys.*, 77:259–315, Apr 2005.
- [24] J. Tobochnik. Properties of the q -state clock model for $q = 4, 5$, and 6. *Phys. Rev. B*, 26:6201–6207, Dec 1982.
- [25] S. R. White. Density matrix formulation for quantum renormalization groups. *Phys. Rev. Lett.*, 69:2863–2866, Nov 1992.
- [26] S. R. White. Density-matrix algorithms for quantum renormalization groups. *Phys. Rev. B*, 48:10345–10356, Oct 1993.